Optics Letters

Multicore fibers with 10 and 16 single-mode cores for the visible spectrum

Saeed Sharif Azadeh,[1,*] Andrei Stalmashonak,[1] Kevin W. Bennett,[2] Fu-Der Chen,[1,3] Wesley D. Sacher,[1] and Joyce K. S. Poon[1,3]

[1]Max Planck Institute of Microstructure Physics, Weinberg 2, 06120 Halle, Germany
[2]Corning Research and Development Corporation, 21 Lynn Morse Rd, Corning, New York 14831, USA
[3]Department of Electrical and Computer Engineering, University of Toronto, 10 King's College Road, Ontario, Toronto, Canada
*Corresponding author: saeed.sharif@mpi-halle.mpg.de

Received 17 October 2021; revised 3 November 2021; accepted 9 November 2021; posted 15 November 2021; published 17 December 2021

We report multicore fibers (MCFs) with 10 and 16 linearly distributed cores with single-mode operation in the visible spectrum. The average propagation loss of the cores is 0.06 dB/m at $\lambda = 445$ nm and < 0.03 dB/m at wavelengths longer than 488 nm. The low inter-core crosstalk and nearly identical performance of the cores make these MCFs suitable for spatial division multiplexing in the visible spectrum. As a proof-of-concept application, one of the MCFs was coupled to an implantable neural probe to spatially address light-emitting gratings on the probe.

https://doi.org/10.1364/OL.446161

Multicore fibers (MCFs) and spatial division multiplexing (SDM) techniques have been investigated extensively, predominantly at telecommunication wavelengths to increase the information capacity of optical fibers [1–4]. Meanwhile, emerging applications in biosensing [5], neuroscience [6–11], and quantum computing [12,13] require photonic integrated circuits (PICs) and optical fibers in the visible spectrum. In these applications, SDM can be leveraged to simultaneously address a plurality of waveguides on the PIC. MCFs can enable such SDM with a single fiber, simplifying the packaging and miniaturizing the form factor. In contrast to imaging fiber bundles [14], MCFs have precisely positioned cores that can be designed to interface with edge or grating couplers on a PIC.

A challenge to MCFs in the visible spectrum is that the core diameters are typically smaller for single-mode (SM) operation compared with telecommunication wavelengths and the mode; hence, inter-core crosstalk may be more sensitive to variations in the core dimensions. Another challenge is that glass fibers have a larger optical loss in the visible spectrum than in the infrared wavelength range. Fortuitously, the near-term applications of visible spectrum MCFs require fibers that are only several meters long, in contrast to the thousands of kilometers required for telecommunications. This eases the requirements of MCF in terms of crosstalk and propagation losses. To the best of our knowledge, an MCF with SM operation for the full visible spectrum has not been reported before.

In this letter, we demonstrate 10- and 16-core MCFs for $\lambda = 445$–640 nm with a one-dimensional distribution of the cores, which is necessary for PIC edge coupling. The uncoupled MCFs are single mode, have low optical losses, low crosstalk, and low bending losses, and the cores exhibit nearly identical characteristics. As a proof-of-concept application, we used a MCF to edge couple to a PIC that is an implantable neural probe, such that each fiber core addressed a light-emitting grating on the probe chip. Implantable neural probes have tight constraints on their form factors; thus, MCFs are ideal to achieve broadband fiber-to-chip coupling and spatial addressing for the probes.

Optical micrographs of the cross section of the homogeneous 10- and 16-core MCFs are shown in Figs. 1(a) and 1(b), respectively. The targeted core-to-core distances (core pitch) were 24 μm and 16 μm. To ease the fabrication process, a step-index profile was chosen, and a moderate refractive index contrast of ~0.005 between the core and cladding was achieved using a 3.4 mol% GeO_2-doped core surrounded by a SiO_2 cladding. Fiber-core canes were produced by the outside vapor deposition (OVD) process, which provides consistent geometric properties and high strength [15]. The OVD process further enables nearly contamination-free glass deposition due to the very tight control of chemicals entering the vapor and thus the glass. A pure silica cladding blank was similarly produced and split into two. The appropriate configuration of holes was drilled in the resulting blanks. The canes were inserted in the holes and fiber was drawn via conventional techniques. As shown in Figs. 1(a) and 1(b), the outer cladding diameter in both MCFs was kept to 300 μm. The MCFs were enclosed in a 100-μm-thick protective coating. For the MCFs to be SM in the visible spectrum, the core diameter of both fibers was set to 2.6 μm with the targeted $1/e^2$ mode field diameter (MFD) of 3.2 μm at $\lambda = 500$nm. This core diameter, which is similar to those of other commercially available single-core SM fibers (e.g., Corning RGB400), results in SM performance of the MCFs in the visible range ($\lambda >$ 400 nm) assuming the aforementioned index contrast, as shown in Fig. 1(c).

The wavelength-dependent refractive indices of the core and cladding are calculated by fitting the Sellmeier equation to the measured refraction values measured at telecom wavelengths, as well as the MFDs measured at discrete wavelengths in the visible range. The simulated and measured MFD values of the

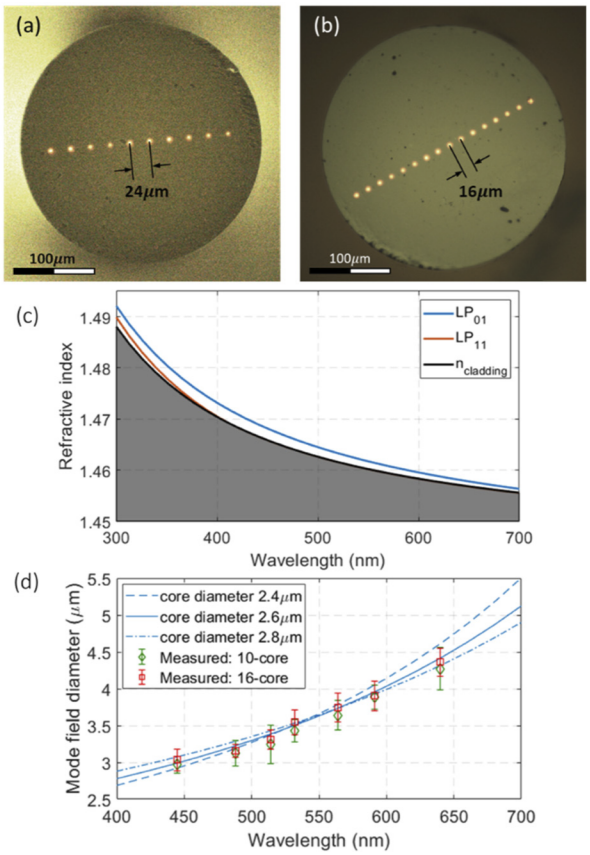

Fig. 1. Micrographs of the (a) 10-core and (b) 16-core MCF facets illuminated with white light. (c) Calculated refractive indices of the lowest-order modes (LP_{01} and LP_{11}). (d) Simulated (lines) and measured (points) mode field diameters of the MCFs in the visible spectrum.

MCF in the visible spectrum are shown in Fig. 1(d), where the blue curves show the calculated MFD for the nominal core size (solid line) and for variations of the core diameter of ± 200 nm (dashed and dotted lines). Although slight variations of the core diameter can reduce the crosstalk due to a change in the relative propagation constant between cores and thus decrease the inter-core coupling, a large MFD can increase the crosstalk at a constant core diameter due to a larger overlap between adjacent modes. We measured the MFDs of the MCFs by coupling light at discrete wavelengths of 445, 488, 514, 532, 564, 591, and 640 nm and recording the output profile at each core using a camera (FLIR GS3-U351S5M).

A high core density, low attenuation, and a large effective area are key characteristics of MCFs for improving the optical signal-to-noise ratio and SDM efficiency [2,16]. To compare the core densities of MCFs, a core multiplicity factor (CMF) was defined in [17] as $\mathrm{CMF} = 4nA_{\mathrm{eff}}/\pi(\mathrm{CD})^2$, where n is the number of cores, A_{eff} is the effective area of the mode, and CD is the cladding diameter. The CMFs of the 10-core and 16-core MCFs at a wavelength of 532 nm with an A_{eff} of 9.5 μm^2 are 1.3×10^{-3} and 2.2×10^{-3}, respectively. The relative CMF (RCMF), which can be defined as the ratio of the CMF of an MCF to that of a standard single-core SM fiber at the same wavelength with an effective core area of 10 μm^2 [2], is 2.63 and 1.65 for the 16-core and 10-core MCFs, respectively. The RCMF is limited by the one-dimensional, linear arrangement of the cores.

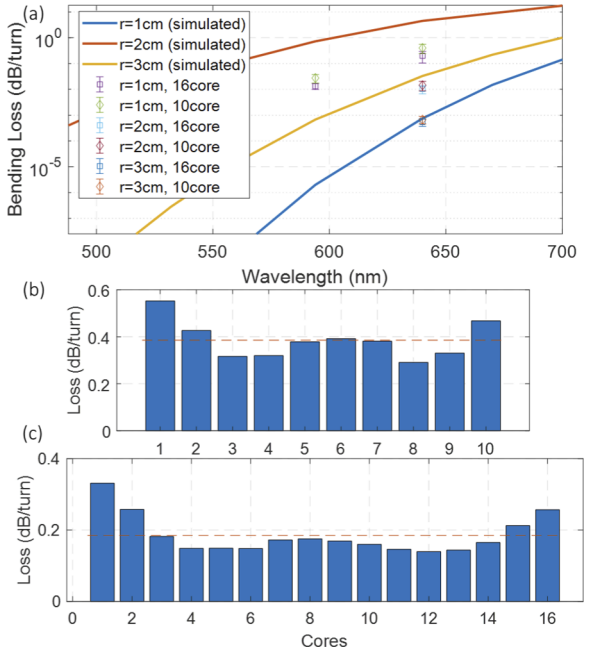

Fig. 2. (a) Calculated and measured bend losses of MCF with different radii. (b), (c) Measured bending losses of individual cores at 640 nm wavelength and a bending radius of 1 cm for (b) 10-core and (c) 16-core MCFs.

The radiative bend losses of the MCFs, calculated using the software Lumerical MODE, are shown in Fig. 2(a) (solid lines) for bend radii of 10, 20, and 30 mm in the visible spectrum. In these simulations, the bend loss was calculated for a single core, and the perfectly matched layers were placed 15 μm from the core center, which is closer than the adjacent core. In this case, any crosstalk due to the bend would manifest as a loss, and the calculated bend loss is independent of the bend orientation, which is an overestimation of the actual bending loss. We measured the bend losses of the MCFs using 20 to 800 turns of MCFs. At λ = 640 nm, the bend losses of the 16-core fiber were $5.5 \times 10^{-4} \pm 1.9 \times 10^{-4}$, 0.01 ± 0.004, and 0.19 ± 0.09 dB/turn, respectively, for bend radii of 3 cm, 2 cm, and 1 cm, whereas we measured $6.7 \times 10^{-4} \pm 2.2 \times 10^{-4}$, 0.014 ± 0.006, and 0.037 ± 0.014 dB/turn for the same radii with the 10-core fiber. At λ = 594 nm and for a radius of 1 cm, the bending losses were 0.013 ± 0.004 and 0.024 ± 0.009 for 16-core and 10-core fibers, respectively. At shorter wavelengths. due to the low bend losses ($<<10^{-3}$ dB/turn), we were unable to measure the loss given the available length of the fiber. In the measurements, the fiber orientation was not kept constant; thus, the measured values represent the bend loss averaged over arbitrary orientations, as would be the case in practical applications of the MCFs. Compared with the simulated losses, the measured values were slightly lower, which is expected due to the aforementioned overestimation of the loss in the simulation. The performance of the fibers was stable at a bend radius of 1 cm after 60 days. The bend losses of individual cores at λ = 640 nm and r = 1 cm are shown in Figs. 2(b) and 2(c), and cores closest to the edge of the fiber have higher losses.

Next, we investigated the core positions of the MCFs. Figure 3 shows the core pitch (here defined as the center-to-center distance relative to the left core) in each MCF, as measured at four different cross-sections separated by at least 20 m. The average core pitches of the 10-core and 16-core MCFs were, respectively,

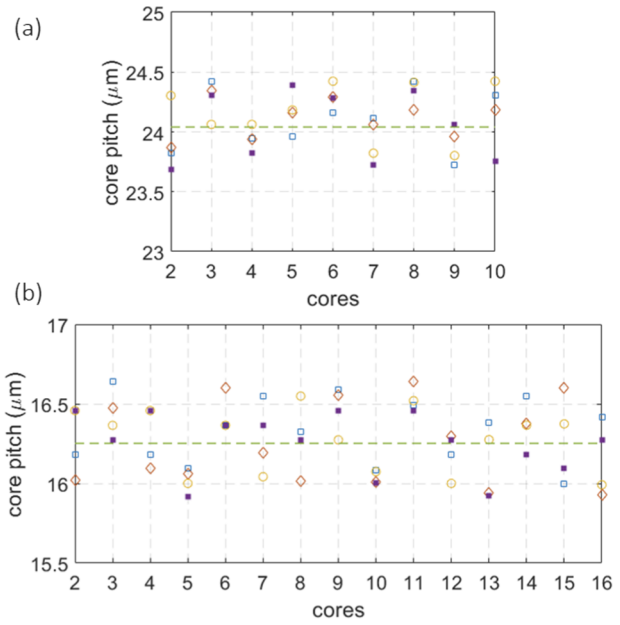

Fig. 3. Core-to-core distances measured at four different facets of the 10-core (a) and 16-core (b) MCFs. The horizontal dashed line in each figure indicates the average core pitch.

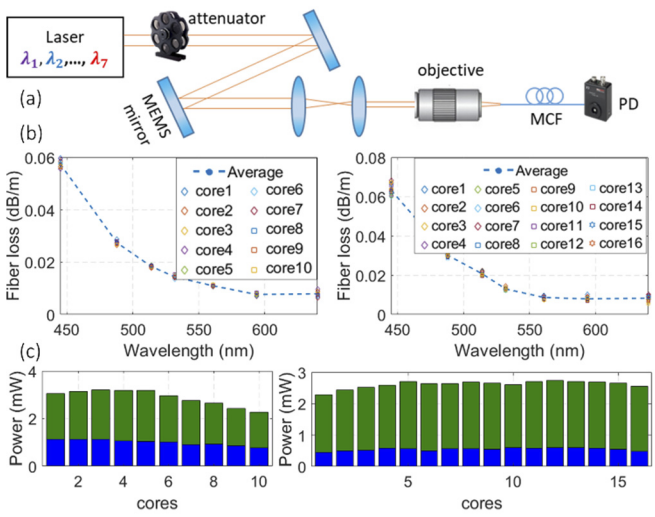

Fig. 4. (a) Cutback measurement setup. (b) Optical losses along the 10-core (left) and 16-core (right) MCFs measured using the cutback method. (c) Comparison of the power transmitted via each individual core at a wavelength of 532 nm (green/light gray bars) and 488 nm (blue/dark gray bars) along a 250-m-long 10-core fiber (left) and a 335-m-long 16-core fiber (right).

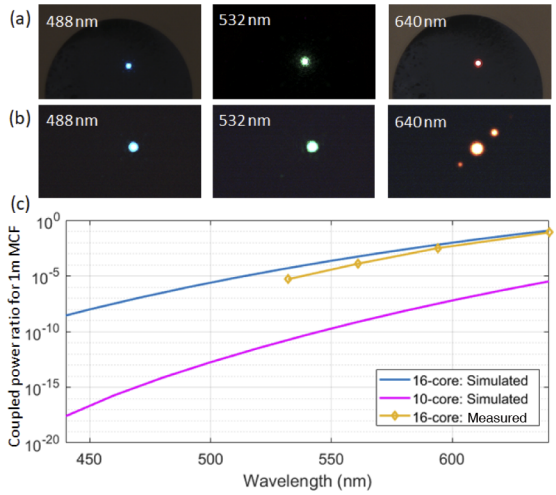

Fig. 5. Images of the output facets of a 250-m-long 10-core fiber (a) and a 5-m-long 16-core fiber (b). (c) Cross-coupled power ratio in 1 m.

24.1 ± 0.3 and 16.3 ± 0.2 μm24.1 and 16.3 μm, with standard deviations of 0.3 and 0.2 μm.

The propagation losses of the fibers were measured using the cutback method. A diagram of the measurement setup is shown in Fig. 4(a). The MCFs were characterized by launching light from laser diodes into each individual core via an objective lens. A computer-controlled micro-electromechanical mirror selected the core to excite. The setup is similar to the one described in [18]. To measure the attenuation of the 10-core MCF, fiber lengths of 10, 20, 50, and 250 m were used. For this MCF, Fig. 4(b) (left) shows that the average propagation loss of the cores was < 0.06 dB/m at 445 nm wavelength and < 0.03 dB/m at wavelengths larger than 488 nm. Cutback measurements of the 16-core MCF were done using fiber sections 10, 20, 40, and 335 m long, and the results are shown in Fig. 4(b) (right). The average propagation losses of the 16-core fiber at wavelengths of 445, 488, 514, and 532 nm were, respectively, 0.063, 0.030, 0.021, and 0.013 dB/m. The loss was less than 0.01 dB/m for wavelengths longer than 561 nm.

The maximum deviation in the loss occurred at 445 nm wavelength and was ± 0.0028 dB/m, which was only 4.5% of the average loss at this wavelength. This deviation was smaller at the other wavelengths for both fibers, and thus we can conclude that the variation in the propagation loss for the cores was within a range of ± 5%. Figure 4(c) shows that the absolute optical powers reaching the end of each core were similar, with slight decreases at the cores that were farther from the center of the MCF. This was expected, since the coupling efficiency (free space to fiber) for the cores near the edge was slightly reduced due to the input beam being off-axis and thus slightly tilted relative to the fiber.

A trade-off exists between core density and crosstalk in uncoupled MCFs. As a rule of thumb [1], if the core-to-core distance between two adjacent cores is less than seven times the core radius, the guided modes become degenerate and the MCF can support the supermodes. Therefore, we investigated the inter-core crosstalk particularly in the 16-core MCF, where the pitch was only ~12 times the core radius. As shown in Fig. 5(a), while no cross-coupled light between the cores at the output facet of the 250-m-long 10-core fiber was observed, the crosstalk became evident at the output of a 5-m-long 16-core fiber (Fig. 5(b)) at longer (red) wavelengths.

We simulated the inter-core crosstalk using coupled mode theory (CMT) [2] for both fibers, assuming the nominal values of the core pitch and diameters. In this simplified CMT model, by neglecting the random fluctuations in the longitudinal direction (z), the cross-coupled power ratio in a pair of straight fibers is simply $P_{cross}/P_0 = F\sin^2(z/2L_c)$, where F is the power conversion efficiency and L_c is the crossover length ($= \pi/2\sqrt{\kappa^2 + (\Delta\beta/2)^2}$, with κ and β the per-length mode coupling and the propagation constant, respectively). In our simulations, $\Delta\beta = 0$ since the fibers are homogeneous MCFs, and

κ is simulated by taking the effective index difference between the even and odd supermodes. The calculated fiber cross-power ratios shown in Fig. 5(c) as blue (top; 16-core) and purple (bottom; 10-core) curves suggest that the cross-coupled power of the 16-core MCF is $\sim 10^5$ times larger than the 10-core MCF at red wavelengths over a 1-m propagation distance.

We characterized the crosstalk by comparing the output power of the adjacent cores using the same setup shown in Fig. 4(a) and replacing the large-area photodetector with a linear camera. Figure 5(c) shows that the worst-case measured cross-coupled power ratios in the 16-core fiber were −53, −39, −25, and −11 dB over 1 m, respectively, at wavelengths of 532, 564, 591, and 640 nm. The measured crosstalk averaged over all cores was −17 dB over 1 m at $\lambda = 640$ nm. The measured crosstalk (yellow curve with diamond symbols) was smaller than the simulated values (blue curve at the top). This discrepancy can be attributed to a larger fabricated core pitch (16.3 μm) than the nominally designed value. Moreover, slight variations of the core diameter, as mentioned, could reduce the coupling coefficient, and thus the cross-coupled power can vary along the MCF. We could not observe or measure the crosstalk in the 10-core fiber at any wavelength; nor that in the 16-core fiber at $\lambda < 532$ nm. Nevertheless, based on the minimum detectable power in our measurement system, and the maximum available length of the fiber, we can determine that the crosstalk was < −65 dB over 1 m in the 10-core and 16-core fibers for $\lambda < 532$nm.

As a proof-of-concept application, Fig. 6 shows the 16-core fiber coupled to a row of edge couplers on a PIC that is an implantable neural probe [9,14]. Neural probes have a tight size constraint for minimal interference with the behavior of the animal under study; thus, an MCF is ideally suited to couple light into multiple inputs on the chip. Each edge coupler was connected to a grating coupler on the shank of the probe. The gratings emit light into brain tissue. Four grating couplers were on the probe shank. The spatial addressing scheme to use such neural probes is described in [9]. The average coupling loss from the fiber to the PIC at $\lambda = 488$ nm was 9.5 ± 0.78 dB. For benchmarking, we measured the coupling loss when the MCF was replaced with a single-core fiber (Nufern S405), which was 9.6 ± 0.5 dB, similar to the MCF and in good agreement with the simulated loss of 8.1 dB. The coupling loss can be reduced with an alternate edge coupler design. Our bilayer design in [19] showed a fiber-to-chip coupling loss of < 4 dB across the visible spectrum with a 1-dB alignment tolerance of about ± 1 μm.

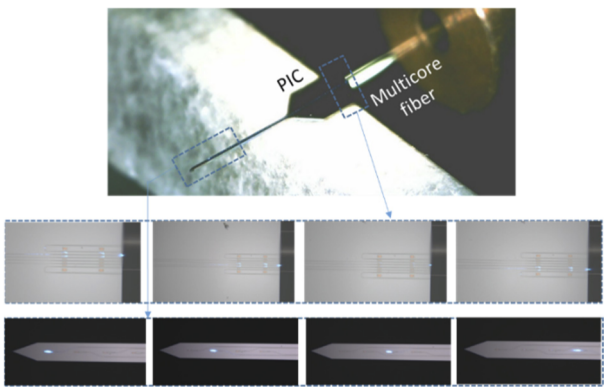

Fig. 6. 16-Core MCF coupled to an implantable neural probe. The top row of insets shows the MCF coupled to a row of edge couplers. The bottom row of insets shows the light emitted from grating couplers, each of which is connected to an edge coupler.

In conclusion, we have demonstrated 10- and 16-core uncoupled MCFs in the visible spectrum with propagation losses of about 0.06 dB/m at 445 nm and < 0.03 dB/m at $\lambda > 488$ nm. While the inter-core crosstalk in the 10-core MCF was < −65 dB over 1 m at $\lambda < 640$ nm, a denser architecture of 16 cores exhibited a larger worst-case crosstalk of −11 dB at $\lambda = 640$ nm. Nevertheless, the worst-case crosstalk of the 16-core fiber was also < −35 dB in 1 m at green and blue wavelengths. The propagation losses as well as the MFD and geometric characteristics were nearly identical for the individual cores in each MCF. As we showed, due to the linear arrangement of the cores and the low losses, low crosstalk, and similar performance of the cores, the use of MCFs to interface with PICs shows promise.

Acknowledgments. The authors are grateful to Alperen Gövdeli for his help on the crosstalk measurements.

Disclosures. The authors declare no conflict of interest.

Data availability. Data underlying the results presented in this paper are not publicly available at this time but may be obtained from the authors upon reasonable request.

REFERENCES

1. A. M. Ortiz and R. L. Sáez, *Multi-Core Optical Fibers: Theory, Applications and Opportunities* (IntechOpen, 2017).
2. Y. Awaji, K. Saitoh, and S. Matsuo, *Optical Fiber Telecommunications VIB: Transmission Systems Using Multicore Fibers* (Elsevier, 2013).
3. K. Saitoh and S. Matsuo, J. Lightwave Technol. **34**, 55 (2016).
4. K. Saitoh, M. Koshiba, K. Takenaga, and S. Matsuo, IEEE Photonics Technol. Lett. **24**, 1898 (2012).
5. M. Porcel, A. Hinojosa, H. Jans, A. Stassen, J. Goyvaerts, D. Geuzebroek, M. Geiselmann, C. Dominguez, and I. Artundo, Opt. Laser Technol. **112**, 299 (2019).
6. L. C. Moreaux, D. Yatsenko, W. D. Sacher, J. Choi, C. Lee, N. J. Kubat, R. J. Cotton, E. S. Boyden, M. Z. Lin, L. Tian, A. S. Tolias, J. K. S. Poon, K. L. Shepard, and M. L. Roukes, Neuron **108**, 66 (2020).
7. S. Libbrecht, L. Hoffman, M. Welkenhuysen, C. Van den Haute, V. Baekelandt, D. Braeken, and S. Haesler, J. Neurophysiol. **120**, 149 (2018).
8. A. Mohanty, Q. Li, M. A. Tadayon, S. P. Roberts, G. R. Bhatt, E. Shim, X. Ji, J. Cardenas, S. A. Miller, A. Kepecs, and M. Lipson, Biomed. Eng. **4**, 223 (2020).
9. W. D. Sacher, F. Chen, H. Moradi-Chameh, X. Luo, A. Fomenko, P. Shah, T. Lordello, X. Liu, I. F. Almog, J. N. Straguzzi, T. M. Fowler, Y. Jung, T. Hu, J. Jeong, A. M. Lozano, P. G. Lo, T. A. Valiante, L. C. Moreaux, J. K. S. Poon, and M. L. Roukes, Neurophotonics **8**, 025003 (2021).
10. E. Segev, J. Reimer, L. C. Moreaux, T. M. Fowler, D. Chi, W. D. Sacher, M. Lo, K. Deisseroth, A. S. Tolias, A. Faraon, and M. L. Roukes, Neurophotonics **4**, 1 (2016).
11. G. Buzsáki, E. Stark, A. Berényi, D. Khodagholy, D. R. Kipke, E. Yoon, and K. D. Wise, Neuron **86**, 92 (2015).
12. K. K. Mahta, C. Zhang, M. Malinowski, T. L. Nguyen, M. Stadler, and J. P. Home, Nature **586**, 533 (2020).
13. R. Niffenegger, J. Stuart, C. Sorace-Agaskar, D. Kharas, S. Bramhavar, C. Bruzewicz, W. Loh, R. Maxson, R. McConnell, D. Reens, G. West, J. Sage, and J. Chiaverini, Nature **586**, 538 (2020).
14. W. D. Sacher, X. Luo, Y. Yang, F. D. Chen, T. Lordello, J. C. C. Mak, X. Liu, T. Hu, T. Xue, P. Guo-Qiang Lo, M. L. Roukes, and J. K. S. Poon, Opt. Express **27**, 37400 (2019).
15. M. G. Blankenship and C. W. Deneka, IEEE Trans. Microwave Theory Tech. **30**, 1406 (1982).
16. K. Imamura, Y. Tsuchida, K. Mukasa, R. Sugizaki, K. Saitoh, and M. Koshiba, Opt. Express **19**, 10595 (2011).
17. K. Takenaga, Y. Arakawa, Y. Sasaki, S. Tanigawa, S. Matsuo, K. Saitoh, and M. Koshiba, Opt. Express **19**, B543 (2011).
18. A. N. Zorzos, J. Scholvin, E. S. Boyden, and C. G. Fonstad, Opt. Lett. **37**, 4841 (2012).
19. Y. Lin, J. C. Mak, H. Chen, X. Mu, A. Stalmashonak, Y. Jung, X. Luo, P. G.-Q. Lo, W. D. Sacher, and J. K. S. Poon, Opt. Express **29**, 34565 (2021).